



The Numerical analysis of an anode-supported high temperature DIR-PSOFC operating conditions with considering the maximum allowable temperature difference

Armin Etemadi^{*1}, Saba Ghorbani¹, Mehdi Masoumpour¹, Mostafa Dadkhah¹, Kazem Atashkari¹

¹Faculty of Engineering, The University of Guilan- Guilan, Iran

PAPER INFO

History:

Received 8 February 2014
Received in revised form
24 April 2014
Accepted 27 September
2015

Keywords:

Numerical Analysis
Fuel cell
SOFC
DIR-PSOFC

ABSTRACT

In the present study, the operating conditions of an anode-supported high temperature direct internal reforming (DIR) planar solid oxide fuel cell (SOFC) are numerically analyzed. SOFCs are the energy conversion devices that produce electricity and heat directly from a gaseous fuel by the electrochemical combination of that fuel with an oxidant. A planar SOFC consists of an interconnect structure and a three-layer region often referred to as the PEN (Positive electrode/Electrolyte/Negative electrode) composed of two ceramic electrodes, anode and cathode, separated by a dense ceramic electrolyte. A 1D mathematical model based on the species and the energy balances is conducted to investigate the concentration of the gas components in the channels and the cell temperature distribution in both solid structures and gas channels. In addition, the electrochemical model of the cell is applied to determine its performance parameters. A synthesis gas with 10% pre-reformed methane as fuel stream is fed to the cell and the water-gas shift, the methane-steam reforming and the electrochemical reactions are considered as mass and heat sources/sinks. The effects of the air ratio and the fuel utilization factor on the temperature field and the performance of the cell are examined through parametric analysis to determine the optimum operating conditions of the cell. The investigations are performed to ensure no cracking will occur due to cell crucial temperature difference. The results indicate that increasing the fuel utilization factor from 0.45 to 0.85 leads to increase the value of the maximum temperature difference across the PEN layer from 101K to 145K while it decreases from 177K to 124K by increasing the air ratio from 6.5 to 12.5. In order to achieve the maximum power density by considering the maximum allowable temperature difference across the cell, the value of the fuel utilization factor and the air ratio are obtained 0.85 and 9, respectively.

© 2015 Published by Semnan University Press. All rights reserved.

1. Introduction

Today, concerns of the environmental and energy crisis, which are due to the rising energy demands, especially in developing countries, result in more attention to the alternative energy conversion methods, e.g. the wind turbines,

geothermal energy, photovoltaic, fuel cells and etc. the Fuel cells, as a promising technology to produce the clean power based on renewable energy resources, have attracted researchers to explore the various aspects of its technology in order to develop it as a feasible and reliable power generation method. The Fuel cells are

^{*}Corresponding author: A.Etemadi, Faculty of Engineering, The University of Guilan- Guilan, Iran. Email: arminetemadi@msc.guilan.ac.ir;

electrochemical devices that produce electricity via electrochemical reactions between fuel and air flows without occurring any combustion and related exergy destructions. Among different types of fuel cells, Solid Oxide Fuel Cell, due to its high operating temperature and capability to work with a wide variety of fuels, appears to be the most appropriate one for power generation purposes, whether using in distributed power generation systems or combining with conventional power plant cycles to improve their efficiencies. From the geometric viewpoint, there are two main types of SOFCs: tubular and planar which are presented in Fig.1. It is necessary to do theoretical investigations where sealing problems and cracking of the solid structure which are due to the high temperature gradients and consequent thermal stresses particularly in power demand fluctuations are probable. Thus, detailed numerical simulations are necessary in order to illuminate the effect of the physical or chemical phenomena that occurring in the gas channels of the Planar SOFCs (PSOFC).

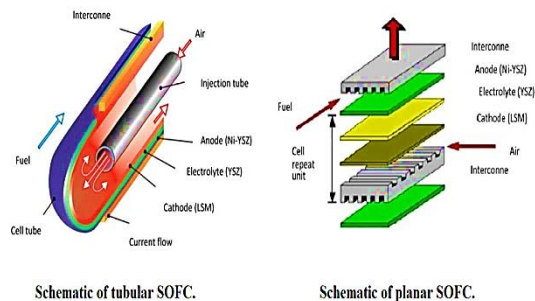


Figure 1. Schematic of tubular and planar SOFCs.

In 1994, Achenbach [1] proposed a three dimensional dynamic modeling of a planar SOFC stack with taking into account the radiation heat transfer mechanism. Moreover, anode gas recycling has also been considered and results indicated the higher plant efficiency and more uniform current density distribution. Ferguson et al [2] investigated the effect of gas channels flow configuration on the planar SOFC performance through a three dimensional modeling. A quasi-two and three dimensional simulation was done by Iwata et al [3] on the mass, the heat and charge transfer in a planar SOFC. Results show an increasing the cell temperature which is due to the fact that increasing the cell power can be controlled by increasing of the operating pressure. Yakabe et al [4] made a computational analysis on momentum and heat transfer of a planar SOFC unit by using syngas as fuel in two cases of external and internal reforming of methane. Their results demonstrated that the internal reforming reaction causes a drop in

temperature at the inlet which produces a tensile stress in electrolyte structure. Aguiar et al [5] made a steady state study on IIR-SOFC modeling by using methane as fuel to find the relation between different reforming catalysts and generated power. The results show that the use of typical metal-based (e.g. Ni) steam reforming catalysts leads to full methane consumption and undesirable local cooling in the first one third of the reformer length. Also Aguiar et al [6] presented the steady state modeling of a planar high temperature anode supported DIR-SOFC by applying syngas as fuel in both co-flow and counter-flow operating conditions. They reported an output voltage of 0.66V, a power density of 0.33Wcm^{-2} , and a fuel efficiency of 47% in case of using a fuel mixture with 10% pre-reformed methane and 75% fuel utilization, inlet fuel and air temperatures of 1023 K, average current density of 0.5Acm^{-2} , and an air ratio of 8.5. In addition, Aguiar et al [7] extended their previous research to a dynamic modeling in order to determine the response of open-loop system against changes in the operating conditions and design appropriate closed-loop system proportional to changes in power demands. Colpan et al [8] analyzed the performance of a planar high temperature anode supported DIR-SOFC thermodynamically by using syngas as fuel. By considering fuel channel gas recirculation, they found that the recirculation ratio has no significant effect power output and electrical efficiency of the cell in case of low current density conditions. Meng Ni et al [9] compared the performance of methane fed planar SOFC with two different types of electrolyte: a) using proton conducting electrolyte and b) using oxygen ion conducting electrolyte, and proved that the latter one has higher performance regardless of previous results, which is due to lower ohm over potential. Jeon et al [10] accomplished a two-dimensional computational modeling of a planar high temperature anode supported SOFC and solved the conservation of ions, mass, momentum and energy equations. As an important point, their results demonstrate that the contribution of potential gain due to temperature rising was considerably high. Iwai et al [11] simulated a planar high temperature anode supported DIR-SOFC numerically to investigate the cell temperature distribution and the local current density. The gas channels are considered as porous media and the analysis was done for the different pre-reforming rates, considering the current density is produced by the carbon monoxide electrochemical reaction. Results illustrate that the current density produced due to hydrogen oxidation is quietly higher than twice of which produced by carbon monoxide.

In the current study, the gaseous components and the temperature distribution of one cell of a

planar anode supported high temperature SOFC is

Table .1. Reactions considered in the mass and energy balances and rate of them		
	Reactions	Rate of reactions
Steam reforming reaction	$CH_4 + H_2O \Leftrightarrow CO + 3H_2$	$\dot{i}_R = z_r \cdot P_{CH_4} \cdot \exp\left(-\frac{E_r}{R_{kj} T_{PEN}}\right)$
Water-gas shift reaction	$CO + H_2O \Leftrightarrow CO_2 + H_2$	$\dot{i}_S = \frac{P_{CO}}{P_{ref}} \left(1 - \frac{(P_{CO_2} \cdot P_{H_2}) / (P_{CO} \cdot P_{H_2O})}{K_{eq,s}}\right)$
Hydrogen oxidation reaction	$H_2 + O^{2-} \rightarrow H_2O + 2e^-$	
Oxygen reduction reaction	$\frac{1}{2}O_2 + 2e^- \rightarrow O^{2-}$	
Overall cell reaction	$H_2 + \frac{1}{2}O_2 \rightarrow H_2O$	$\dot{i}_{elec} = \frac{j}{2F}$

numerically investigated. The governing equations including mass fractions for the fuel and air flow in gas channels and also energy balances in the domain are solved numerically along with the appropriate boundary conditions by using a numerical procedure through a code using MATLAB in order to determine the mass fractions and the temperature distribution in the gas channels and solid structures. The main advantage of the present work is that the thermal conductivity of the fuel and air components are function of their temperature in gas channels and are not considered to be constant. In order to prevent the emergence of severe thermal gradient and to find out optimal operating condition, the effects of the SOFC operating conditions on the temperature field during the cell are investigated.

2. Mathematical model

In this study, 1D steady-state solid oxide fuel cell has been developed. A complete solid oxide fuel cell is not only consisting of a single cell, but also the several cells, which are connected both in series and/or in parallel. The developed model includes the mass, thermal and electrochemical analysis, as well as the kinetic models of hydrocarbon reactions. Also the pressure drop along the cell channel is assumed to be zero [6].

For the purpose of modeling, it is considered that the SOFC is composed of the fuel and air channels and of the electrochemical region represented by anode, electrolyte, and cathode. The air which has been comprised of O_2 and N_2 is considered as cathode channel reactant and 10% pre-reformed methane with steam to carbon 2 is considered as fuel for anode channel. Two types of chemical reactions (methane reforming and water - gas shift reaction) occur at the anode while the cells are supplied with the natural gas because the cell operating temperature was sufficiently high [12].

Table 1 presents the cell reactions and the rate of them.

2.1. Mass balance

Both air and fuel flows are assumed to be steady and laminar. The Molar fluxes in the gas channels are considered to be convective in flow direction and the gas flow in the same direction. Mass balances are derived in plug-flow form along the longitudinal direction, because of high Peclet numbers [6]. By Applying the Faraday's law, the rates of the electrochemical reactions are related to the electric current [1] which can be expressed by:

$$\dot{i}_{elec} = \frac{j}{2F} \quad (1)$$

Steam reforming and water-gas shift reactions occur on the anode surface. The reaction rates for steam reforming and water-gas shift reactions are calculated from Achenbach [1] and Aguiar [6]

$$\dot{i}_R = z_r (P_{CH_4}) \cdot \exp\left(-\frac{E_r}{R_{kj} T_{PEN}}\right) \quad (2)$$

$$\dot{i}_S = \left(\frac{P_{CO}}{P_{ref}}\right) \cdot \left(1 - \frac{(P_{CO_2} \cdot P_{H_2}) / (P_{CO} \cdot P_{H_2O})}{K_{eq,s}}\right) \quad (3)$$

where $z_r = 4.274 \text{ mol / (bar.m}^2\text{.s)}$, $E_r = 8.2 \times 10^4 \text{ kJ / kmol}$ and $K_{eq,s}$ is the equilibrium constant for shift reaction which is expressed by

$$K_{eq,s} = \exp\left(-\frac{g_{H_2}^0 + g_{CO_2}^0 - g_{CO}^0 - g_{H_2O}^0}{R_{kj} T_{PEN}}\right) \quad (4)$$

The mass balance equation for air channel can be written as

$$V_{ac} \frac{\partial \rho_{O_2}}{\partial x} = - \frac{\dot{i}_{elec} \cdot M_{O_2}}{h_{ac}} \quad (5)$$

And for the fuel channel can be written as

$$V_{fc} \frac{\partial \rho_i}{\partial x} = - \frac{(v_{i,k} \dot{i}_k) \cdot M_i}{h_{fc}} \quad (6)$$

$$i \in \{CH_4, H_2O, CO, H_2, CO_2\},$$

$$k \in \{elec, R, S\}$$

Where $\nu_{i,k}$ is the stoichiometry coefficient of component i in reaction k . And the boundary conditions are

$$x = 0 \begin{cases} \rho_{O_2} = \rho_{in} \\ \rho_i = \rho_{in} \end{cases}, \quad i \in \{CH_4, H_2O, CO, H_2, CO_2\} \quad (7)$$

2.2. Energy balance

In a fuel cell, the current and temperature distributions are strongly coupled. Therefore, knowledge of the predominant heat transfer processes is required. Heat transfer processes include heat release from electrochemical reactions, electrical resistances, convective heat transfer between cell components and fuel and air gas streams, heat conduction through cell components and radiation between solid parts.

Energy balance has to be established for the fuel and air flows and the solid structure separately. It is assumed that all reaction enthalpies are released at the electrode/electrolyte interfaces or at three phase boundaries (TPB). Therefore, the reaction enthalpies appear in the source terms of the solid structure balances.

The energy balances for the gas flows include the convective heat transfer from channel walls to the gas and heat capacity of the gases with respect to their composition. Thermal flux in the PEN and interconnector structures is conductive. And due to the high temperatures, radiation heat transfer between PEN and interconnect structures is taken into account. It is assumed that the cell is in the center of a stack, so there is no heat transfer through the external walls. Thus the energy balances are calculated through Eqs. (8)–(11).

Air channel

$$V_{ac} \rho_a C_p a \frac{\partial T_a}{\partial x} = h_{a,PEN} (T_{PEN} - T_a) \frac{1}{h_{ac}} + h_{a,int} (T_{int} - T_a) \frac{1}{h_{ac}} \quad (8)$$

Fuel channel

$$V_{fc} \rho_f C_p f \frac{\partial T_f}{\partial x} = h_{f,PEN} (T_{PEN} - T_f) \frac{1}{h_{fc}} + \quad (9)$$

$$h_{f,int} (T_{int} - T_f) \frac{1}{h_{fc}} - \dot{r}_r \Delta H_r \frac{1}{h_{fc}} - \dot{r}_s \Delta H_s \frac{1}{h_{fc}}$$

PEN structure

(10)

$$K_{PEN} \frac{\partial^2 T_{PEN}}{\partial x^2} = h_{f,PEN} (T_{PEN} - T_f) \frac{1}{t_{PEN}} + h_{a,PEN} (T_{PEN} - T_a) \frac{1}{t_{PEN}} \\ + \varepsilon_{cr} \sigma F_{cr,int} (T_{PEN}^4 - T_{int}^4) \frac{1}{t_{PEN}} + \varepsilon_{an} \sigma F_{an,int} (T_{PEN}^4 - T_{int}^4) \\ + (j_{avg} E) \frac{1}{t_{PEN}} + \dot{r}_{elec} \Delta H_{elec}$$

Interconnector

$$K_{int} \frac{\partial^2 T_{int}}{\partial x^2} = h_{f,int} (T_{int} - T_f) \frac{1}{t_{int}} + h_{a,int} (T_{int} - T_a) \frac{1}{t_{int}} \\ - \varepsilon_{cr} \sigma F_{cr,int} (T_{PEN}^4 - T_{int}^4) \frac{1}{t_{int}} \\ - \varepsilon_{an} \sigma F_{an,int} (T_{PEN}^4 - T_{int}^4) \frac{1}{t_{int}} \quad (11)$$

And the boundary conditions are written as

$$x = 0 \begin{cases} T_a = T_{in} \\ T_f = T_{in} \end{cases} \quad (12)$$

$$x = 0, x = L \begin{cases} \frac{\partial T_{PEN}}{\partial x} = 0 \\ \frac{\partial T_{int}}{\partial x} = 0 \end{cases} \quad (13)$$

Heat transfer coefficients between gas channels and solid structures were calculated by using a constant Nusselt number of 3.09 [6] and the channel hydraulic diameter. Therefore, these coefficients are expressed by

$$h_{ac,PEN} = h_{ac,int} = Nu \frac{K_{air}}{D_{H,ac}} \quad (14)$$

$$D_{H,ac} = \frac{2W h_{ac}}{W + h_{ac}}$$

$$D_{H,fc} = \frac{2W h_{fc}}{W + h_{fc}} \quad (15)$$

$$h_{fc,PEN} = h_{fc,int} = Nu \frac{K_{fuel}}{D_{H,fc}}$$

Where K_{air} and K_{fuel} are the thermal conductivity of air and fuel flow, respectively.

2.3. Electrochemical model

The reversible output voltage of the SOFC is expressed by the Nernst equation [1] as a function of the Gibbs free energy change during electrochemical reaction. This is called open circuit voltage of the cell:

$$E^{OCV} = -\frac{\Delta G^0}{2F} + \frac{RT}{2F} \ln \left(\frac{P_{H_2} \cdot P_{O_2}^{1/2}}{P_{H_2O}} \right) \quad (16)$$

where ΔG^0 is the Gibbs free energy change from reactants to products ($J.mol^{-1}$), $F=96485.3$ is the Faraday constant ($C.mol^{-1}$), $R=8.314$ is the universal gas constant ($J.mol^{-1}.K^{-1}$), T is the electrochemical reaction temperature (K) and P_{H_2} , P_{O_2} and P_{H_2O} are the reacting gas pressures (atm) of hydrogen, oxygen and vapor, respectively. ΔG^0 is expressed by:

$$\Delta G^0 = G_{H_2O}^0 - (G_{H_2}^0 + \frac{1}{2}G_{O_2}^0) \quad (17)$$

$$G_{specie}^0 = H_{specie}^0 - T.S_{specie}^0 \quad (18)$$

Where $G_{H_2O}^0$, $G_{H_2}^0$ and $G_{O_2}^0$ are the Gibbs free energy ($J.mol^{-1}$) of vapor, hydrogen and oxygen respectively. H_{specie}^0 is the corresponding enthalpy ($J.mol^{-1}$) and S_{specie}^0 is the corresponding entropy ($J.mol^{-1}.K^{-1}$). The gas enthalpy and entropy is calculated by referring to the JANAF Table [13]. Reversible voltage is the maximum potential that can be produced by a cell under specific operating conditions. Actually, the output voltage of the cell, due to over potentials, is lower than the reversible voltage and can be calculated from Eq. (19):

$$E = E^{OCV} - (\eta_{ohm} + \eta_{conc,anode} + \eta_{conc,cathode} + \eta_{act,anode} + \eta_{act,cathode}) \quad (19)$$

Where η_{ohm} is ohmic loss and $\eta_{conc,anode}$, $\eta_{conc,cathode}$, $\eta_{act,anode}$ and $\eta_{act,cathode}$ are the anode and cathode concentration and activation overpotential losses, respectively.

2.4. Overpotentials

Ohmic, concentration and activation overpotentials are the three types of losses that occur during the operation of the cell. Definitely, the ohmic loss is defined as the resistance of the cell solid structures against the conduction of ions and electrons which is expressed by:

$$\eta_{ohm} = jR_{ohm} \quad (20)$$

Where j is the current density and R_{ohm} is the internal resistance of the cell, which contains electronic and ionic resistances. R_{ohm} is written as

$$R_{ohm} = \frac{\tau_{anode}}{\sigma_{anode}} + \frac{\tau_{cathode}}{\sigma_{cathode}} + \frac{\tau_{electrolyte}}{\sigma_{electrolyte}} \quad (21)$$

Where τ_{anode} , $\tau_{cathode}$ and $\tau_{electrolyte}$ are thickness of anode, cathode and electrolyte, respectively. Also σ_{anode} and $\sigma_{cathode}$ are electronic conductivities of the anode and cathode, and $\sigma_{electrolyte}$ is ionic conductivity of the electrolyte [6].

Concentration overpotential is the other loss in the cell performance, which is produced due to the difference between species partial pressures in the channel flow and three phase boundary (TPB). In order to occurring electrochemical reaction that occurs on the TPB, the gaseous species must diffuse through porous electrodes which called Knudsen diffusion. In addition, each species should diffuse through the other species via bulk diffusion. Due to these facts, the values of the local concentration species on the TPB differ with their values in the bulk fuel flow and, consequently, the species partial pressures in the Nernst Equation should be rewritten for TPB which expressed in Eq. (22).

$$E_{TPB}^{OCV} = E_{H_2}^0 + \frac{RT}{2F} \ln \left(\frac{P_{H_2,TPB} \cdot P_{O_2,TPB}^{1/2}}{P_{H_2O,TPB}} \right) \quad (22)$$

The difference between Eqs. (16) and (22) produces the concentration overpotential

$$\eta_{conc} = \frac{RT}{2F} \ln \left(\frac{P_{H_2O,TPB} \cdot P_{H_2,fuelchannel}}{P_{H_2O,fuelchannel} \cdot P_{H_2,TPB}} \right) + \frac{RT}{4F} \ln \left(\frac{P_{O_2,airchannel}}{P_{O_2,TPB}} \right) \quad (23)$$

Where, the first and the second terms on the right hand side are anodic and cathodic concentration overpotentials, respectively.

Partial pressure of water, hydrogen and oxygen at the three- phase boundary can be calculated by

$$P_{H_2,TPB} = P_{H_2,fuelchannel} - \frac{RT \tau_{anode}}{2FD_{eff,anode}} j \quad (24)$$

$$P_{H_2O,TPB} = P_{H_2O,fuelchannel} + \frac{RT \tau_{anode}}{2FD_{eff,anode}} j \quad (25)$$

$$P_{O_2,TPB} = P - (P - P_{O_2,airchannel}) \exp \left(\frac{RT \tau_{cathode}}{2FD_{eff,cathode} P} j \right) \quad (26)$$

Where $\overline{D_{eff,anode}}$ and $D_{eff,cathode}$ are average effective diffusivity coefficients at anode and cathode, respectively and D_{eff} is written as

$$D_{eff,i} = \frac{\varepsilon_p}{\tau_{tortuosity}} D_{molecular,i} \quad (27)$$

$i \in \{H_2, H_2O, O_2, N_2\}$

ε_p is the material porosity and $\tau_{tortuosity}$ is tortuosity factor. $D_{molecular,i}$ is expressed by

$$\frac{1}{D_{molecular,i}} = \frac{1}{D_{bulk,i}} + \frac{1}{D_{knudsen,i}} \quad (28)$$

$i \in \{H_2, H_2O, O_2, N_2\}$

Bulk diffusivity, $D_{bulk,i}$ is caused by fluid–fluid intermolecular collisions as considered by the kinetic theory of gases. Knudsen diffusivity $D_{knudsen,i}$ is the result of fluid-wall collisions, when the pore size is so small that it is less than the mean path of the fluid.

Activation overpotential is extra potential necessary to defeat the energy barrier and transfer an electron between electronic the ionic conductors. This overpotential reflects the kinetics involved with the electrochemical reactions.

The activation overpotential is expressed by the Butler-Volmer equation

$$j = j_{0,electrode} \left[\exp \left(\frac{\alpha n F}{RT} \eta_{act,electrode} \right) - \exp \left(- \frac{(1-\alpha)nF}{RT} \eta_{act,electrode} \right) \right] \quad (29)$$

$electrode \in \{anode, cathode\}$

Where α is the transfer coefficient (usually $\alpha = 0.5$) [9], n is the number of electrons participating in electrochemical reaction and $j_{0,electrode}$ is the exchange current density, expressed as

$$j_{0,electrode} = \frac{RT}{nF} k_{electrode} \exp \left(- \frac{E_{electrode}}{RT} \right) \quad (30)$$

$electrode \in \{anode, cathode\}$

Where $k_{electrode}$ and $E_{electrode}$ values are presented in the Table 2.

3. Result and discussion

The anode supported design is the most favorable one for SOFC [14], therefore this study is carried out on an anode support solid oxide fuel cell with internal reformer. In order to verify the results, the obtained results are compared with the data from Aguiar[6] which is represented in table 4. Gas composition and temperature profile of each layer show s an acceptable agreement with Aguiar's results. The comparison between Aguiar's results and the present work with constant thermal conductivity is presented in Fig.2. Range of parameters involved in this modeling and default values of geometry and operating condition of fuel cell are given in table 3.

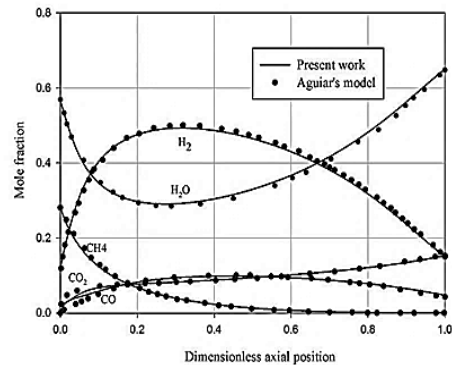
The simulated results of current-voltage characteristic are shown in Fig.3. As it can be seen, the cathode activation overpotential has a significant magnitude in comparison with other overpotentials. Anode activation overpotential and ohmic loss are the next reasons causing the voltage drop.

Fig.4 shows the magnitude of overpotential in fuel cell. The vertical axis shows overpotential and horizontal axis shows three operating temperatures: 973, 1023 and 1073. At 973K, activation overpotential accounted for 72.5% and concentration overpotential accounted for only 3% of the total of losses as mentioned in the legend.

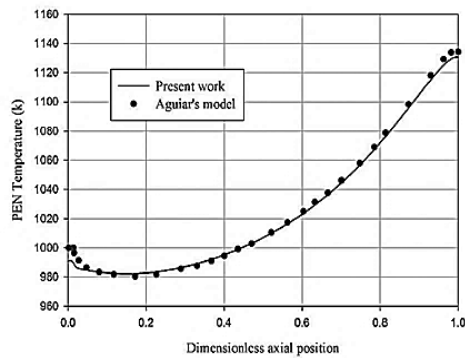
Also, these results show that the amount of over potential decreases by increasing the work temperature. At 973K, overpotential contribution will be increased to 9.3%.

Table2. Data for exchange current density equation

	k	E
Cathode	$2.35 \times 10^{11} \Omega^{-1} m^{-2}$	137 KJ mol^{-1}
Anode	$6.54 \times 10^{11} \Omega^{-1} m^{-2}$	140 KJ mol^{-1}



(a)



(b)

Figure 2. Comparison of Aguiar's result and present work for (a) Mole fraction of fuel components and (b) PEN temperature

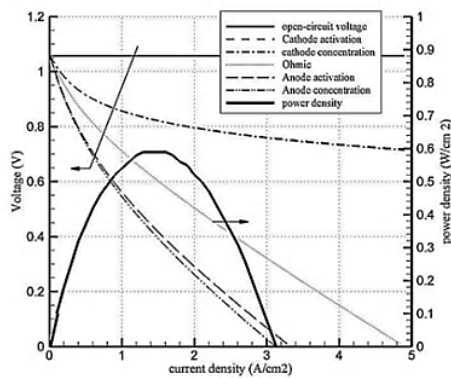


Figure 3. Cell voltage and power density as a function of current density at 1023K for a totally reformed fuel mixture

Table3. the operating and geometrical parameters used in the mathematical model

Geometrical parameter	Value	Operating parameter	Value
Cell length (m)	0.4	Air and fuel input temperature (°K)	1024
Cell width (m)	0.1	Air and fuel input pressure (bar)	1
Fuel and air channel height (mm)	1	Average current density (A/cm ²)	0.5
Anode thickness (μm)	500	air ratio	8.5
cathode thickness (μm)	50	Fuel utilization	75%
electrolyte thickness (μm)	50	steam / carbon	2.
interconnect thickness (μm)	500	pre reforming rate	10%

3.1. Gas composition and temperature distribution

Fig.5 illustrates temperature curves of each layer along fuel cell length. The Cell temperature falls steadily in the initial part of a fuel cell as a result of the sharply endothermic reforming reaction, as expected. In Fig.6, distributions of reforming and shift reaction rates are shown. It can be seen that by reducing the influence of reforming reaction, the temperature will raise over the cell.

Fig.7 shows the mole fraction distribution in the fuel channel. The mole fraction of water and methane at the beginning of the cell are prominent because the steam reforming reaction is dominant. As a result of reforming, the concentration of hydrogen and monoxide carbon will rise gradually and the concentration of methane and water will be reduced. To put it more simply, 80 percent of the input methane will be consumed in 22% of the elementary input cell and hydrogen molar fraction will be more than doubled. But due to the electrochemical reaction, the hydrogen

concentration near the outlet reduces and the concentration of water will be increased.

3.2. Effect of air ratio

The Air ratio is one of the most effective parameters for controlling the cell temperature and preventing the occurrence of a temperature gradient. The Inlet air flow rate is adjusted to keep maximum temperature difference across the fuel cell lower than 150K [15]. Values of the maximum PEN temperature difference in the air ratio between 6.5 and 12.5 are presented in Table 5.

Figs. 8 and 9 show the effect of this parameter on the temperature and local current density distribution across the cell. Increasing of the air ratio will decrease the temperature difference throughout the channel and current density distribution becomes more uniform. But it should be considered that at high pressure, increase in the work of the compressor and the cycle efficiency will eventually come down. Hence it is necessary to choose it carefully.

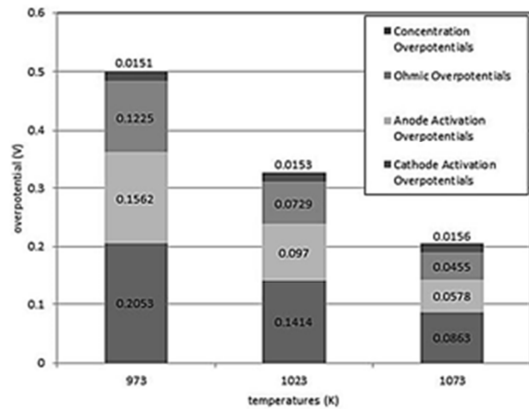


Figure 4. The Magnitude of overpotential in the fuel cell at three operating temperatures: 973, 1023 and 1073

Table4. The comparison results obtained with Aguiar [6]

Parameter	Aguiar [2]	Present
Output voltage (V)	0.66	0.65
PEN temperature (°K)		
min	980	985
max	1134	1138
Fuel Channel temperature (°K)		
min	970	981
max	1127	1135
Interconnect temperature (°K)		
min	976	983
max	1120	1131
Local current density		

(A/m ²)	2385	2751
min	9385	8517
max		

Table 5. PEN temperature difference for SOFC model of Figs 2 and 3

Air ratio	temperature difference(°K)
6.5	177.8
8.5	154.1
10.5	127.2
12.5	110.1

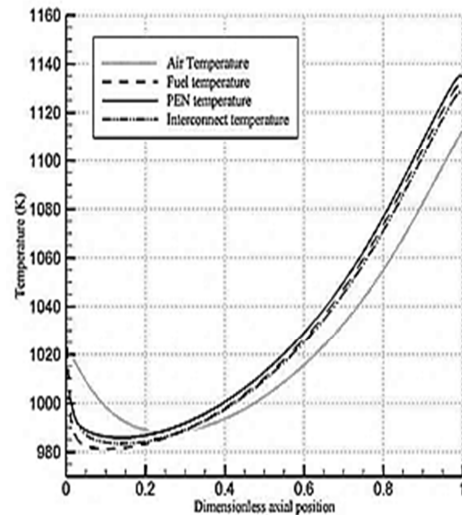


Figure 5. Fuel and air channels, PEN structure, and interconnect temperature along the cell length for the conditions in Table 2

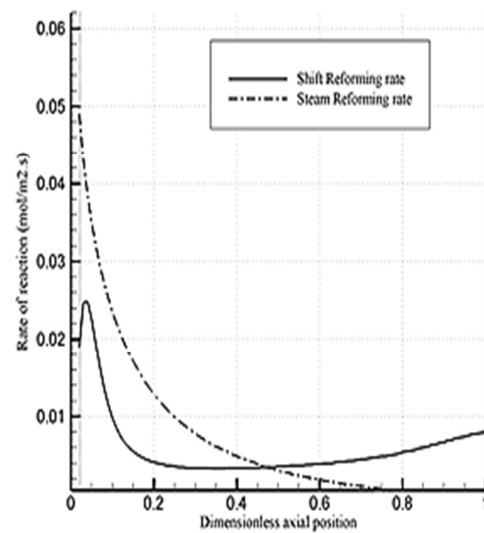


Figure 6. The distributions of thereforming and shift reaction rates

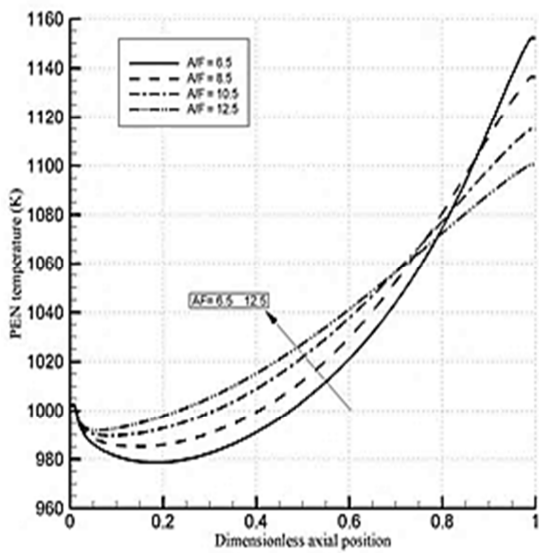


Figure 8. The Effect of air ratio on the PEN temperature curves

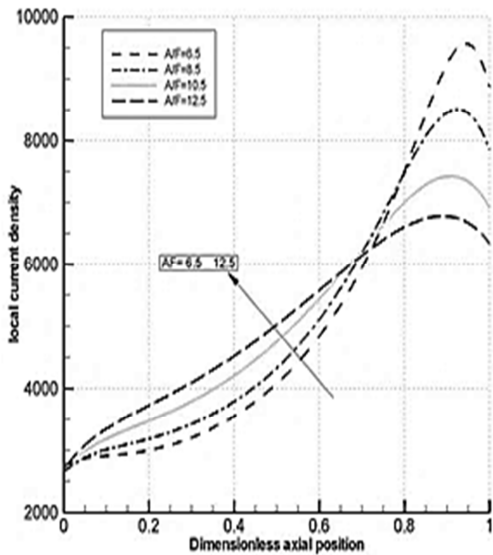


Figure 9. The Effect of air ratio on the local current density

3.3. Effect of fuel utilization factor

Figs 10 and 11 illustrate the effect of changing fuel utilization. Fuel utilization factor is the ratio of fuel consumed to produce electricity to the total amount of inlet fuel. Fig 8 presents the PEN temperature profile along the cell. It indicates that temperature will rise gradually with increase of the utilization factor. As a result of increasing temperature, the activation loss (that causes major losses in the fuel cell) will be reduced. Thus, the

operating voltage and subsequently power density will be increased.

In general, by increasing this parameter power density will be increased, but the excessive increase of fuel utilization factor causes reduction in the amount of hydrogen in the terminal of cell and consequently the concentration over potential will be increased. Also in high fuel utilization, the temperature difference is higher due to unbalanced current density distribution in the cell.

4. Conclusions

In this study, an anode-supported high-temperature DIR-SOFC fed by 10% pre-reformed methane is studied. This model considers the mass transport and heat transfer, over potentials and ohmic loss which the heat transfer process is based on the exothermic and endothermic reactions occurring in fuel channel. The model can effectively predict the distribution of each layer temperature curve, current density and gas molar fraction along the channels.

A parametric analysis was performed to investigate the effects of some operational parameters on temperature difference across the cell. The investigations indicate that the temperature difference grows from 101K to 145K by increasing the fuel utilization factor from 0.45 to 0.85 and deduces from 177K to 124K by increasing the air ratio from 6.5 to 12.5. Because of the fact that the cell power density can be dwindled by increasing the anode activation loss which itself is temperature dependent, the maximum power density by considering the maximum allowable cell temperature difference is considered as objective and the values of the fuel utilization factor and air ratio are obtained 0.85 and 9, respectively.

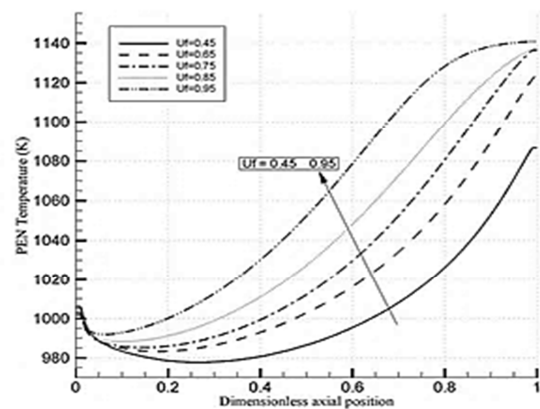


Figure 10. The Effect of fuel utilization factor on the

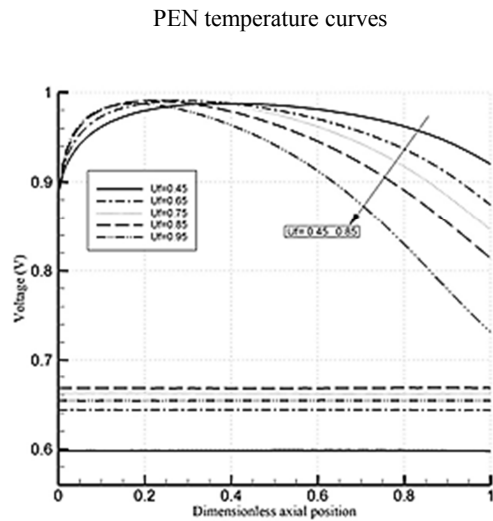


Figure 11. The Effect of fuel utilization factor on the operating voltage and open-circuit potential

Nomenclature

C_p	specific heat capacity	(kJ kg ⁻¹ K ⁻¹)
D_H	hydraulic diameter of a rectangular cross section gas channel	(m)
D_{bulk}	bulk diffusivity coefficient	(m ² s ⁻¹)
D_{eff}	effective diffusivity coefficient	(m ² s ⁻¹)
$D_{kmudsen}$	molecular diffusivity coefficient	(m ² s ⁻¹)
$D_{molecular}$	Knudsen diffusivity coefficient	(m ² s ⁻¹)
E	Potential	(V)
E^{OCP}	open-circuit potential	(V)
$E_{electrode}$	activation energy of the exchange current density	(kJ mol ⁻¹)
F	Faraday's constant	(C mol ⁻¹)
h_{ac}	air channel height	(m)
h_{fc}	fuel channel height	(m)
h_{ct}	heat transfer coefficient for cathode	(kJm ⁻² s ⁻¹ K ⁻¹)
h_{an}	heat transfer coefficient for anode	(kJm ⁻² s ⁻¹ K ⁻¹)
j	local current density	(Am ⁻²)
\bar{j}_{avg}	average current density	(Am ⁻²)
$\bar{j}_{0,electrode}$	exchange current density	(Am ⁻²)
K	thermal conductivity	(kJm ⁻¹ s ⁻¹ K ⁻¹)
$k_{electrode}$	pre-exponential factor of the exchange current density	(Am ⁻²)
n	number of electrons participating in the electrochemical reaction	
Nu	Nusselt number	
P	pressure	(Pa)
P_i	partial pressure of component i	(Pa)
$P_{i,TPB}$	partial pressure of component i at three phase boundary	(Pa)

\dot{r}_i	rate of reaction i	(molm ⁻² s ⁻¹)
R_{kj}	gas constant	(kJ mol ⁻¹ K ⁻¹)
R_{ohm}	total cell resistance, including both ionic and electronic resistances	(Ωm ²)
T	temperature	(K)
V_{ac}	air velocity	(ms ⁻¹)
V_{fc}	fuel velocity	(ms ⁻¹)
W	system width	(m)
α	transfer coefficient	
ΔH_{elec}	enthalpy change of the electrochemical reaction	(kJ mol ⁻¹)
ε_p	electrode porosity	
σ	Stefan-Boltzmann constant	(Wm ⁻² K ⁻⁴)
σ_{anode}	electronic conductivity of the anode	(Ω ⁻¹ m ⁻¹)
$\sigma_{cathode}$	electronic conductivity of the cathode	(Ω ⁻¹ m ⁻¹)
$\sigma_{electrolyte}$	ionic conductivity of the electrolyte	(Ω ⁻¹ m ⁻¹)
ρ	Density	(kgm ⁻³)
τ	thickness	(m)
$\tau_{tortuosity}$	Tortuosity	

References

- [1] Achenbach, E., Three-dimensional and time-dependent simulation of a planar solid oxide fuelcell stack. J Power Sources, 49 (1994) 333–48.
- [2] Ferguson, J.R., Fiard, J.M., Herbin, R., Three-dimensional numerical simulation for various geometries of solid oxide fuel cells. J Power Sources 58 (1996) 109–22.
- [3] Iwata, M., Hikosaka, T., Morita, M., Iwanari, T., Ito, K., Onda, K., et al., Performance analysis of planar-type unit SOFC considering current and temperature distributions, Solid State Ionics, 132 (2000) 297-308.
- [4] Yakabe, H., Ogiwara, T., Hishinuma, M., Yasuda, I., 3-D model calculation for planar SOFC. J Power Sources, 102 (2001) 144–54.
- [5] Aguiar, P., Chadwick, D., Kershenbaum, L., Modeling of an indirect internal reforming solid oxide fuel cell, Chem. Eng. Sci. 57 (2002)1665–1677.
- [6] Aguiar, P., Adjiman, C.S., Brandon, N.P., Anode-supported high temperature direct internal reforming solid oxide fuel cell. I: modelbased steady-state performance. J Power Sources, 138 (2004) 120–36.
- [7] Aguiar, P., Adjiman, C.S., Brandon, N.P., Anode-supported high temperature direct internal reforming solid oxide fuel cell: II. Modelbased dynamic performance and control. JPower Sources, 147 (2005) 136–47.
- [8] Colpan, C.O., Dincer, I., Hamdullahpur, F., Thermodynamic modeling of direct internal reforming solid oxide fuel cells operating with syngas. J Hydrogen Energy, 32 (2007) 787-795.

- [9] Meng, N.i., Dennis, Y.C., Leung, M., Leung, K.H., Modeling of methane fed solid oxide fuel cells: Comparison between proton conducting electrolyte and oxygen ion conducting electrolyte *J Power Sources* 183 (2008) 133–142.
- [10] Dong HyupJeon A comprehensive CFD model of anode-supported solid oxide fuel cells. *Electrochimica Acta*, 54 (2009) 2727–2736.
- [11] Iwai, H., Yamamoto, Y., Saito, M., Yoshida, H., Numerical simulation of hightemperaturedirect-internal-reforming planar solid oxide fuel cell. *Energy*, (2011) 1–10.
- [12] Singhal, S.C., Kendall, K., High temperature solid oxide fuel cells: fundamentals, design and applications. Oxford: Elsevier; (2003) 12–7.
- [13] Chase, M.W., NIST-JANAF thermochemical tables, fourth edition, *J. Phys. Chem. Ref. Data*, Monograph, 9 (1998) 1–1951.
- [14] Meng, Ni., YC Leung, D., KH Leung, M., Electrochemical modeling and parametric study of methane fed solid oxide fuel cells. *J Energy Conversion and Management*, 50 (2009) 268- 278.
- [15] Bove, R., Ubertini, S., *Modeling Solid Oxide Fuel Cells: Methods, Procedures and Techniques*. 2008: Springer.